Check for updates

Original research article

I·M3 Institute of Materials, Minerals & Mining

Science and Technology of Welding and Joining
1–11
© The Author(s) 2026
Article reuse guidelines:
sagepub.com/journals-permissions
DOI: 10.1177/13621718261472548
journals.sagepub.com/home/stw

Sage

Tandem gas metal arc welding of thick steel plates: Progress in productivity and properties using advanced process modes

Prashant Kumar Chaurasia[1,2], Çağtay Fabry[2], Andreas Pittner[2], Amitava De[3] and Michael Rethmeier[2,4,5]

Abstract

Tandem gas metal arc welding (T-GMAW) utilizes simultaneous deposition from two wires to enhance the productivity for joining thick sections. Current knowledge on the actual energy consumption vis-à-vis filler wire deposition rate in T-GMAW is limited. We present here a detailed investigation on multi-pass single V-groove T-GMAW of a 30 mm thick structural steel plate with real-time monitoring of current, voltage and metal transfer modes for both filler wires. A novel electrical deposition efficiency (EDE) metric is realized using measured current and voltage transients to correlate electrical energy usage with the deposition rate. For a constant wire feed rate, the short-circuiting metal transfer mode resulted in much lesser energy input and 50% higher EDE in comparison to the pulsed mode of metal transfer.

Keywords

tandem gas metal arc welding, electrical deposition efficiency, energy efficiency, environmental impact, real-time monitoring, cooling time, hardness, steel

Received: 2 May 2026; accepted: 7 July 2026

Introduction

The increasing demand for sustainable and energy-efficient manufacturing has positioned the tandem gas metal arc welding (T-GMAW) as an emergent joining technology for thick sections.[1–4] T-GMAW can help enhance the welding travel speed (WTS),[5] deposition rate and energy utilization in comparison to the single-wire GMAW,[6] which is limited by lower energy efficiency,[2,3] deposition rate and productivity.[4] A quantitative understanding of the influence of the process variables for two filler wires on the weld joint quality in T-GMAW is currently lacking.[7] An assessment of the energy utilization vis-à-vis filler wire deposition rate in T-GMAW in comparison to that in single-wire GMAW is rarely reported.[5] The key motivation of the present work is therefore a quantitative understanding of the actual electrical energy utilization vis-à-vis the filler wire deposition rate, and the achievable joint quality in T-GMAW process in comparison to that in single-wire GMAW.

The single-wire GMAW process embodies limited wire feed rate (WFR), typically up to 20 m/min.[2] In contrast, T-GMAW employs two filler wires concurrently with independent control to improve deposition rate, process efficiency, and joint properties.[3,4] Fang et al.[4] found a good process stability and productivity at a comparatively low energy input for T-GMAW. T-GMAW with pulsed and short-circuiting modes of metal transfer, respectively for the leading and trailing filler wires, was found a possible recourse[8] albeit the synchronization challenge for two metal transfer modes.[3,5] The control of current pulses for two filler wires to ensure the droplet transfer stability revealed the need for advanced power source control.[2,3] T-GMAW provided around 20% reduction in energy consumption and 50% decrease in welding time compared to single-wire GMAW but the process stability in T-GMAW was found critical.[2] Applications of T-GMAW are evolving for the joining of thick sections in steel,[9] aluminium,[10,11] and high-strength steel.[12–14] The aforementioned studies, especially refs,[2,3] examined the energy consumption in T-GMAW using the prescribed process settings with the available power sources that allowed at limited control on the selection of WFR and metal transfer mode of individual filler wires. A detailed quantitative assessment of the energy utilization based on individual control of the leading and trailing filler wires, and associated real-time monitoring of current, voltage,

[1]Department of Engineering Science, University West, Trollhättan, Sweden
[2]Division 9.3 - Welding Technology, Bundesanstalt für Materialforschung und –prüfung (BAM), Berlin, Germany
[3]Mechanical Engineering Department, Indian Institute of Technology Bombay, Mumbai, India
[4]Joining Technology Department, Technische Universität Berlin, Berlin, Germany
[5]Joining and Coating Technology, Fraunhofer IPK, Berlin, Germany

Corresponding author:
Prashant Kumar Chaurasia, Department of Engineering Science, University West, Trollhättan 46186, Sweden.
Email: prashant-kumar.chaurasia@hv.se

WFR and metal transfer modes has remained in ever demand for T-GMAW.

T-GMAW uses a greater volume of filler wire material implying a higher carbon footprint for the fabrication of thick sections, and a quantitative assessment of the actual energy consumption vis-à-vis filler wire deposition rate is required but currently scarce. We present here a comprehensive experimental investigation on T-GMAW of a thick steel section with real-time monitoring of current and voltage transients, and WFR and metal transfer modes. A unique electrical deposition efficiency (*EDE*) metric is estimated to correlate the actual energy usage with the filler wire deposition rate for both pulsed current and short-circuiting modes of metal transfers in T-GMAW and compared with that for the single-wire GMAW. The transverse cross-sections of the weld joint specimens are monitored using a laser scanner that has helped encompass the weaving width and ensure defect-free inter-layer weld profile. The microhardness distribution on the weld cross-sections is measured and correlated with the recorded cooling time ($t_{8/5}$).

Experimental set-up and methodologies

An integrated T-GMAW setup with synchronised leading and trailing power sources (Fronius TPS-500i), a six-axis robot (YASKAWA-AR1730 with YRC1000 controller) and an in-situ monitoring system (Beckhoff TwinCAT3)[15] is used. The schematic experimental setup is shown in Figure S1 in the supplemental document. The current and voltage transients, and the WFR are monitored at a sampling rate of 10 Hz.[15] The net input power (P_P) is estimated as the summation of the arc powers for the leading and trailing wire as[2,3]

$$P_P = P_{PL} + P_{PT} = \frac{1}{t}\left[\left\{\int_0^t V(t)\,.\,I(t).dt\right\}_L + \left\{\int_0^t V(t)\,.\,I(t).dt\right\}_T\right] \quad (1)$$

where $V(t)$ and $I(t)$ are the instantaneous voltage and current values. The net arc power input (P_P) is averaged over a finite time period (t) with 100 cycles for each condition.[15–17] The energy input per unit length of weld for the leading (E_L) and trailing (E_T) wires are estimated as (P_{PL} / v) and (P_{PT} / v), respectively, where v is the WTS. The net energy input (E) per unit length of weld is calculated as (P_P / v) and the energy consumption in terms of *EDE* (in g/kWh) is estimated as

$$EDE = \left[\frac{v_{wL} + v_{wT}}{P_{PL} + P_{PT}}\,\rho\left(\frac{\pi}{4}d_w^2\right)\right] = \left[\frac{v_w}{P_P}\,\rho\left(\frac{\pi}{4}d_w^2\right)\right] \quad (2)$$

In equation (2), ρ is the density of filler wire material, d_w is the wire diameter, v_{wL} and v_{wT} are the measured leading and trailing WFR, respectively, and v_w is the total WFR, i.e., $v_w = v_{wL} + v_{wT}$. Thus, *EDE* provides an estimate of the utilized energy in terms of the deposited mass per kWh of energy consumption. Since *EDE* is estimated using the filler wire diameter (d_w), and the measured WFR and arc power (P_P), the *EDE* remains invariant to the geometric orientation of the torch and local curvature of the deposited bead profile.

Figure 1(a) to (c) shows the welding torch configuration, the multi-pass joint design, and the weaving strategy, respectively. Both wires are set at an angle of 4° with their individual vertical axes (Figure 1(a)). The joints were made in flat position (1G) with a forward torch configuration with respect to the leading wire to ensure adequate melting and penetration. Figure 1(b) shows the transverse sectional view of the joint with one root pass and five filling passes. The root pass is filled by the leading wire only. A ceramic backing plate is used to support the molten metal during root pass and restrict heat loss. The base plates are tack-welded along their edges to minimize misalignment due to warpage. Figure 1(c) shows the thermocouple (TC_{1-3}) locations and the sinusoidal weaving strategy.[2] The weaving strategy was employed for the root pass and the filling passes. The corresponding weaving amplitude and frequency for all the passes are presented in Table 1. The weaving amplitude and frequency are selected according to the groove geometry for each pass to ensure side-wall and inter-pass fusion, and groove filling. The contact tip to workpiece distance (CTWD) for each filling pass is set based on the previously deposited pass profile.

Table 1 shows five T-GMAW conditions (W1–W5) that are used to obtain a combination of pulsed current (PMC: *pulse multi control*) and short-circuiting (CMT: *cold metal transfer*) modes of metal transfer at varying weld pass parameters. The W1 and W3 conditions involve PMC mode of metal transfer for both leading and trailing wires but the weld parameters for individual passes are different. In contrast, both W2 and W4 conditions embody PMC mode metal transfer for the leading wire and CMT mode of metal transfer for the trailing wire with different weld pass parameters. Lastly, the W5 condition considers CMT mode of metal transfer for the both the leading and trailing wires. Overall, these five T-GMAW conditions (W1–W5) provide an opportunity to realize the influence of the metal transfer mode and the weld pass parameters on the energy usage, filler wire deposition rate, and weld joint quality. In Table 1, WFR_{TO} is the summation of the leading and trailing wire WFR.

One K-type thermocouple (TC_4 in Figure 1(b)) was used to measure the layer-wise critical cooling time ($t_{8/5}$) between 800–500°C, which was placed dynamically during each pass just behind the arc at the mid-length. The manual insertion of TC_4 resulted in a little variation in the local monitoring location within a range of around 2–4%. However, its effect on the measured values of $t_{8/5}$ was found to be minimal. The thermocouples TC_1, TC_2 and TC_3 (Figure 1(c)) were fixed on the top surface of the plate to monitor the preheat temperature between 100–150°C. In turn, the thermocouples TC_1–TC_3 provide thermal cycles at points on the top surface just beside the groove, and TC_4 provides the thermal cycle of the melt pool at the mid-length of each pass during cooling. The shielding gas (ISO14175:M21:Ar-18%CO_2) flow rate is kept constant at 20 L/min for each wire. The weld coupons are prepared using a 30 mm thick structural steel base plate and 1.2 mm diameter ER70S-6 filler wire, and their chemical compositions are shown in Table S1 in the supplemental document.

The inter-layer weld profiles are monitored using a laser line triangulation (LLT) scanner (Micro-Epsilon

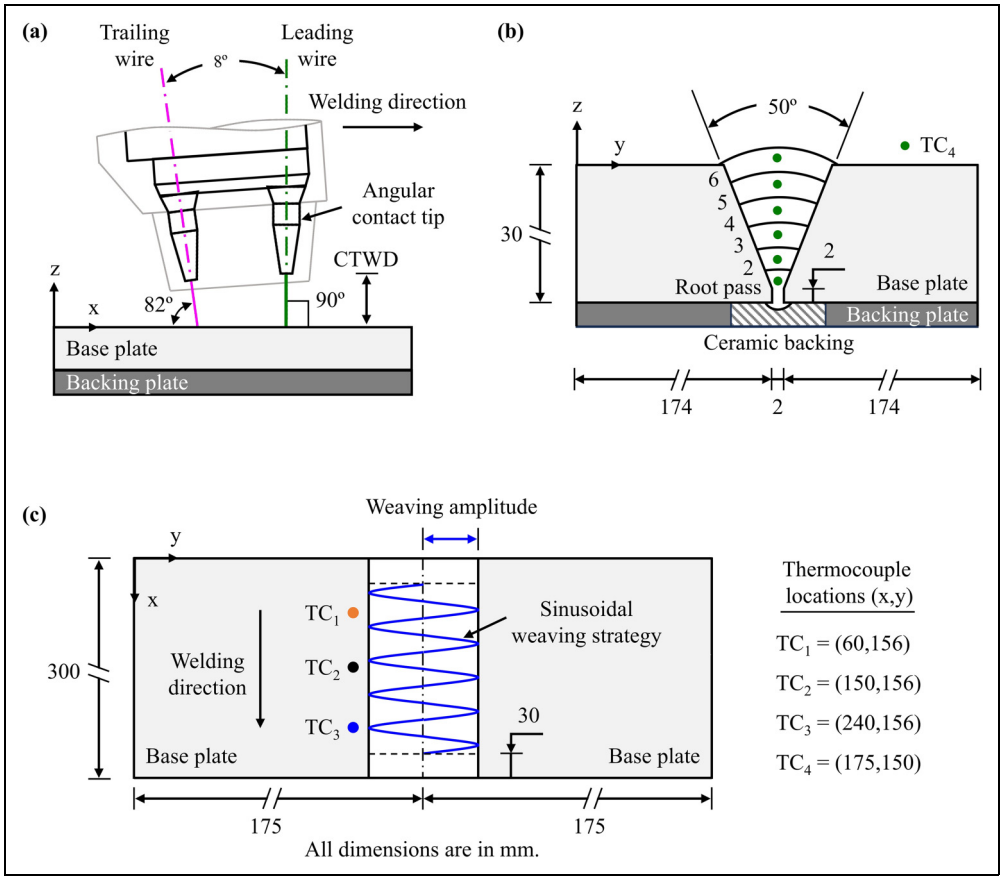

Figure 1. Schematic of (a) T-GMAW torch orientation, (b) six-pass weld groove design, and (c) weaving strategy and thermocouple (TC) locations for T-GMAW of thick steel plates.

LLT3010-100) at a 0.05 mm resolution along the laser line.[15] Each pass profile is considered to set the weaving amplitude and CTWD for the next pass to minimize the lack-of-fusion defect. Two samples are extracted from the mid-length, polished and etched with Nital solution (2%) to view the transverse cross-sections under an optical microscope (Axio Imager-M2m). The measured weld cross-sections are mapped with the corresponding laser-scanned pass profiles to identify the root penetration and inter-pass fusion. The spatial distribution of Vickers microhardness across weld cross-sections is measured with a two-dimensional grid spacing of 0.20 mm. A list of abbreviations and variables is presented in Table S2 in the supplemental document.

Results and discussion

This section presents first the measured current and voltage transients, and the estimated arc power and *EDE* for the second to sixth filling passes. The weld pass cross-sections are presented next followed by the measured cooling time ($t_{8/5}$) and 2D spatial microhardness mappings.

Monitored current, voltage and arc power transients

Figure 2(a) shows the current, voltage and arc power transients for the W3 condition for both the filler wires with pulsed (PMC) mode of metal transfer, which shows an in-phase synchronization of the pulse-on and pulse-off durations of the two wires. The pulse-on period exhibits a higher value of current, voltage and arc power in comparison to that in the pulsed-off duration.[16] In contrast, Figure 2(b) shows a mixed nature of the current, voltage and arc power transients for the W4 condition with the leading wire in pulsed (PMC), and the trailing wire in short-circuiting (CMT) modes of metal transfer. A much higher arc power is noted for the pulsed (PMC) mode, which is also reported earlier.[16–18] Figure 2(c) presents the current, voltage and arc power transients for the W5 condition for both the filler wires in the short-circuiting (CMT) metal transfer mode. A comparison of Figure 2(a) to (c) shows a much higher arc power for the pulsed (PMC) mode in comparison to the short-circuiting (CMT) mode of metal transfer.

The metal transfer in pulsed (PMC) mode is characterized with the rapid melting of filler wire tip and detachment of fine droplets during the pulse-on period due to peak pulse current, whereas the pulse-off period maintains a relatively low-power arc with a much lower current and arc voltage.[16] However, the time-averaged current, voltage and arc power still remain considerably significant due to very high peak current and arc voltage, albeit for a small pulse-on time.[16–18] In contrast, the metal transfer in the advanced short-circuiting (CMT) mode is driven by a controlled forward and retraction oscillating motion of the filler wire at a high frequency as the molten filler wire tip touches the melt pool creating a short-circuit.[19–21] The overall low-energy arcing and controlled short-circuiting result in a notably smaller time-averaged current, and arc voltage and power in this advanced short-circuiting (CMT) metal transfer mode.[22]

Table 1. Process conditions used for T-GMAW of V-groove butt welds.

Condition	Layer	WFR_L	WFR_T	WFR_{TO}	WTS	Weaving amplitude	Weaving frequency	CTWD
[L; T]		m/min	m/min	m/min	mm/s	mm	Hz	mm
W1: [L: PMC; T: PMC]	1	12.5	–	12.5	6.67	0.65	2.5	28
	2	15	12.5	27.5	10	1.5	1.4	23.5
	3	20	15	35	7	5.5	0.8	20
	4	20	15	35	6.33	8	0.6	20
	5	20	15	35	5.33	10	0.5	20
	6	12.5	8	20.5	3	11.75	0.3	20
W2: [L: PMC; T: CMT]	1	12.5	–	12.5	6.67	0.65	2.5	28
	2	15	12	27	10	1.5	1.4	23.5
	3	20	12	32	7	5	0.8	20
	4	20	12	32	6.33	7.5	0.6	20
	5	20	12	32	5.33	10	0.5	20
	6	12.5	8	20.5	3	11.75	0.33	20
W3: [L: PMC; T: PMC]	1	12	-	12	6.67	0.65	2.5	28
W4: [L: PMC; T: CMT]	2	12	12	24	10	4.5	1.4	23.5
W5: [L: CMT; T: CMT]	3	12	12	24	7	6.5	1	20
	4	12	12	24	6.33	8.9	1	20
	5	12	12	24	5.33	11	0.7	20
	6	12	12	24	3	12.25	0.8	20

PMC: *Pulse multi control*; CMT: *Cold metal transfer*; WFR: wire feed rate; L: leading; T: trailing; WTS: welding travel speed; CTWD: contact tip to workpiece distance.

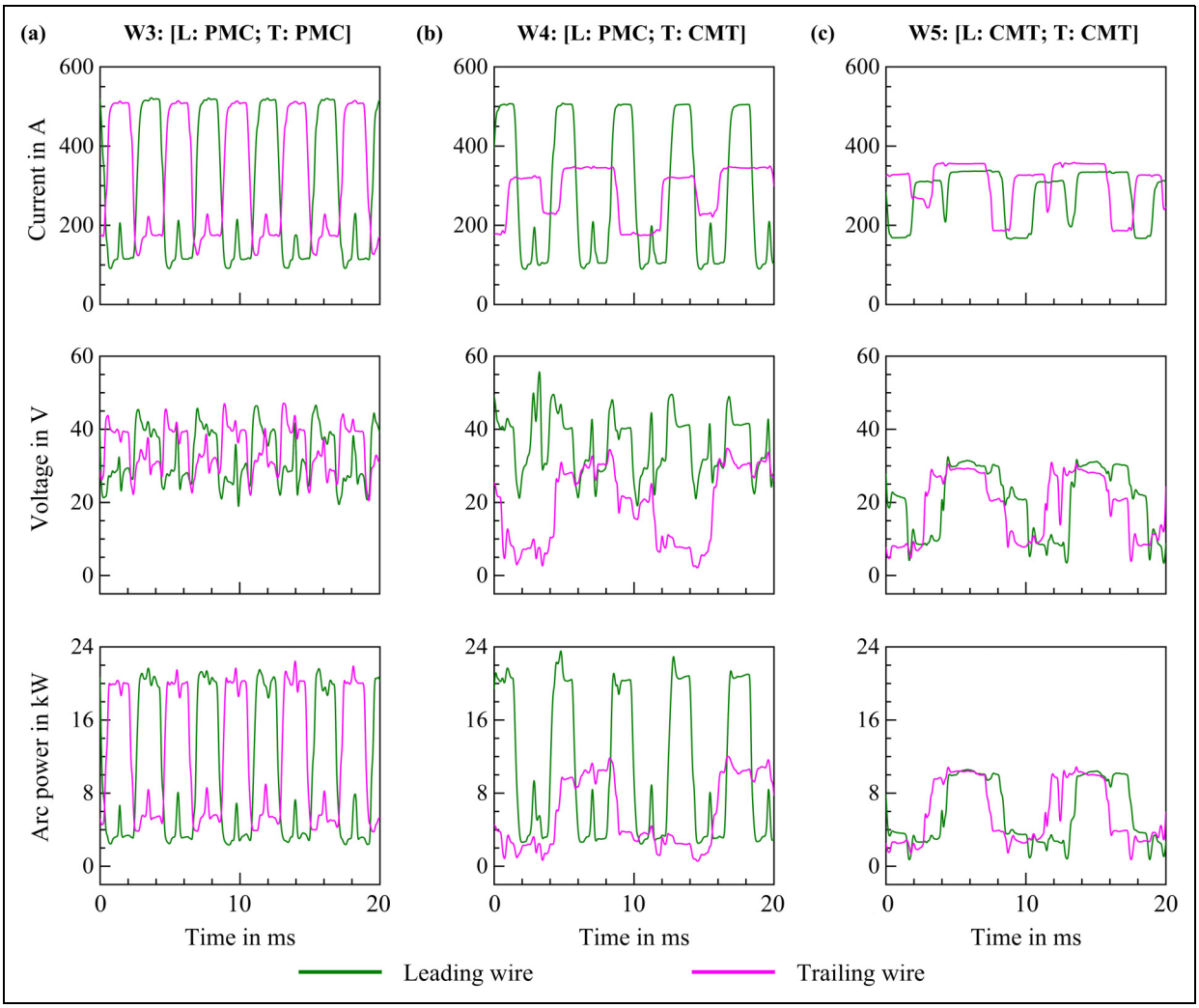

Figure 2. Current, voltage and arc power transients during third pass for (a) W3 [L: PMC; T: PMC], (b) W4 [L: PMC; T: CMT] and (c) W5 [L: CMT; T: CMT] welding conditions (Table 1). Other welding conditions are: WFR_L = 12 m/min, WFR_T = 12 m/min, WTS = 7 mm/s.

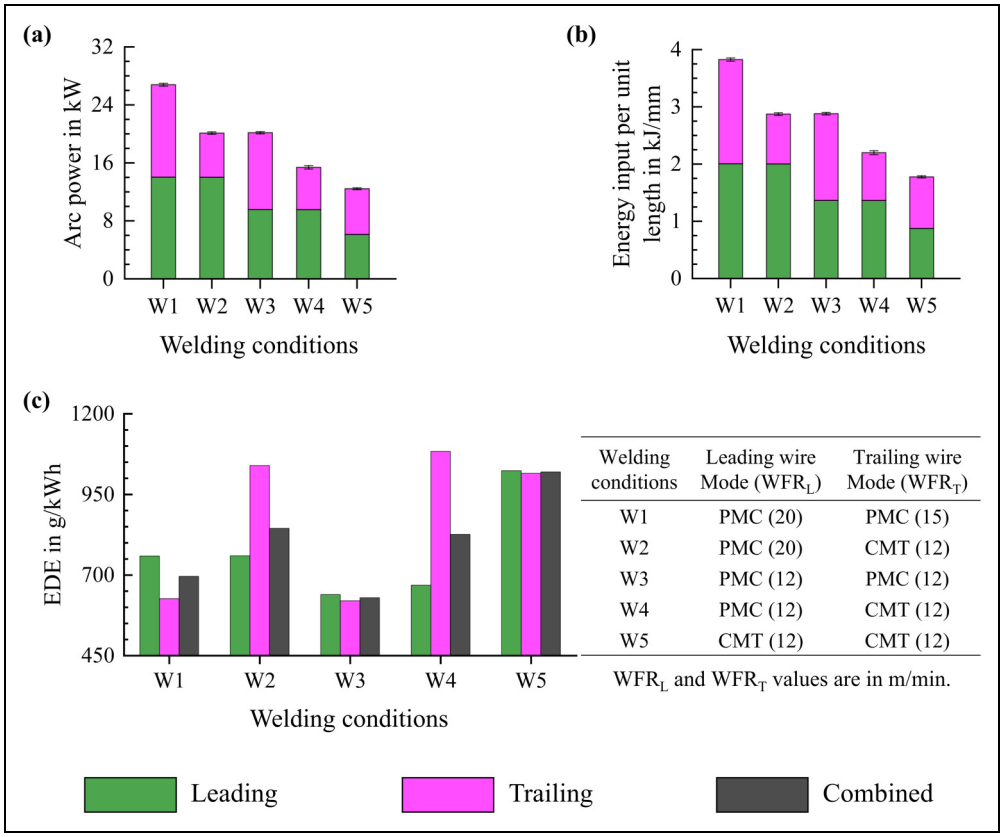

Figure 3. Estimated (a) arc power, (b) energy input per unit length, and (c) electrical deposition efficiency (EDE) during the third weld pass for five welding conditions (Table 1).

Estimation of average power and EDE

The current, voltage and arc power transients for the individual weld passes are used to study the nature of influence of the metal transfer mode and weld pass parameters, WFR and PTS, on the time-averaged arc power, energy input and the *EDE*. Figure 3(a) presents the measured values of leading (P_{PL}) and trailing (P_{PT}) wire arc powers, and the net process power (P_P) during the deposition of the third pass for five welding conditions. The third pass is chosen as a representative example. Figure 3(a) shows higher leading and trailing wire arc powers for the W1 condition than for W3 condition albeit with pulsed (PMC) mode of metal transfer for both wires, which is attributed to higher WFR in W1 condition. Likewise, the trailing wire arc power in W2 condition is found greater than that in W4 although both employ short-circuiting (CMT) metal transfer mode, which is also attributed to higher WFR for the W2 condition. A comparison of the arc powers for the W3, W4 and W5 conditions shows the highest arc power for W3 followed by those for W4 and W5 conditions. Although these three conditions employ the same WFR, the pulsed (PMC) metal transfer mode for both wires in W3 condition has resulted in the highest arc power.

Following the arc power variations in Figure 3(a), the corresponding leading (E_L) and trailing (E_T) wire arc energy inputs are plotted in Figure 3(b). For the same WTS of 7 mm/s, the net energy input is the highest for the W1 condition, which is attributed to high WFR and pulsed (PMC) mode of metal transfer. The trailing (E_T) wire energy input reduces slightly for the W2 condition due to short-circuiting (CMT) metal transfer mode and a lesser WFR. A smaller WFR for both wires reduce the net energy input further for the W3 condition. The minimum energy input is attained for the W5 condition, which is attributed to the short-circuiting (CMT) metal transfer mode for both wires. In summary, Figure 3(b) shows that a smaller WFR and in particular, the short-circuiting (CMT) metal transfer mode reduce the energy input significantly during the T-GMAW process.

The energy deposition efficiency (*EDE*) is estimated using equation (2), and the combined *EDE* for the T-GMAW setup is evaluated as the ratio of the total WFR ($WFR_L + WFR_T$) and the net arc power, P_P i.e., ($P_{PL} + P_{PT}$). Figure 3(c) shows a higher leading wire *EDE* than the trailing wire for W1 condition, which is attributed to higher WFR, and the combined *EDE* presents a mean of the leading and trailing wire *EDE* values. Figure 3(c) further shows a higher trailing wire *EDE* for W2 condition, which is attributed to smaller arc power and implies an improved energy utilization in short-circuiting (CMT) metal transfer mode. The net *EDE* of W2 condition is much higher than that for W1. A higher arc power and energy input result in a smaller *EDE* for W3 condition with both wires in pulsed (PMC) mode, implying a reduced deposition per kWh of energy consumption. A comparison of the *EDE* values for W3 and W5 conditions reinforces the superiority of the short-circuiting (CMT) mode for a greater rate of filler wire deposition per kWh energy consumption. With both wires in CMT mode, the W5 condition results in a notably higher *EDE* compared to W3 even with the same WFR.

It is noteworthy that the calculated *EDE* is directly proportional to the measured WFR (v_w) and inversely

proportional to the estimated arc power (P_P) as shown in equation (2). The arc power (P_P) was estimated over around hundred real-time current and voltage transients, and the WFR (v_w) was also examined over a similar number of real-time measured values for each pass. The deviations in the measured WFR (v_w) and the estimated arc power (P_P) were found to be well within a range of 1 to 2%, resulting in a similar range of deviation in the calculated *EDE* value for each pass. A similar procedure is repeated for each pass over all the welding conditions, W1 to W5. In Figures 2 and 3, the measured values of voltage and current transients, and the estimated values of arc power, energy and *EDE* are shown only for the third pass of the five welding conditions, W1 to W5, for consistency. Similar results for other passes for the five welding conditions, W1 to W5, are not plotted again for brevity and reducing the repetition of plotting of similar results. However, the *EDE* values for all the weld passes, and conditions are presented in Table S3 in supplemental document.

It is noteworthy that Figure 3(c) presents the *EDE* values for the third filling pass to highlight the direct influence of selected metal transfer mode and WFR. However, an overall representation of the net *EDE* values for each welding condition is of interest for productivity and energy usage, which are considered important for actual applications. Figure 4(a) shows a generalized representation of *EDE* as a function of productivity (WFR) and energy consumption (arc power). The estimated *EDE* values of second to sixth passes for the W1 to W5 conditions are shown as a function of the combined WFR_{TO} for each case. For W1 and W2 conditions, WFR_{TO} is different for second and sixth passes, and the same for the third to fifth passes (Table 1). For W3 to W5 conditions, WFR_{TO} is the same for all second to sixth passes (Table 1). For the range of WFR_{TO}, 20.5–35 m/min, *EDE* is much lower for W1 and W3 conditions with both the wires in PMC mode. The CMT mode of metal transfer for both the wires in W5 condition results in much higher *EDE*, even with a lower WFR_{TO} of 24 m/min. The CMT mode of metal transfer for only the trailing wire (W2 and W4) increases *EDE* by around 25% compared to both wires with PMC mode (W1 and W3).

Figure 4(b) presents an overall process-level comparison of the achievable range of *EDE* in T-GMAW based on the values obtained in this work and that reported in contemporary literature,[2,3] rather than identifying a single best or worst condition. In other words, Figure 4(b) aims at providing a comparative process window as a result of continuous advancements of welding processes and power sources. The *EDE* values in Figure 4(b) are calculated as an average of the *EDE* values of all the filling passes for welding conditions with similar metal transfer modes. Accordingly, the *EDE* values for W1 and W3 are combined and shown as the first bar pair (L: PMC, T: PMC), those for W2 and W4 are combined for the second bar pair (L: PMC, T: CMT), and W5 is shown separately as both the wires are in short-circuiting metal transfer mode (L: CMT, T: CMT).

With both the wires in PMC mode of metal transfer (L: PMC, T: PMC), the average *EDE* value are aligned with those reported in the literature,[2,3] for a similar range of combined WFR between 20–35 m/min. A little improvement in *EDE* in the present work is attributed to the enhanced control of current and voltage transients in the newer generation of T-GMAW power sources. With the leading wire in PMC mode and the trailing wire in CMT mode (L: PMC, T: CMT), the average *EDE* value is improved by 25% in the present work, which is attributed to the increase in the range of combined WFR from 17–27 m/min^2 to 20–32 m/min. Likewise, for both the wires in advanced short-circuiting (CMT) mode (L: CMT, T: CMT), the average *EDE* is improved by around 26% in the present work as the range of the combined WFR could be increased from 14–16 m/min^{2,3} to 24 m/min in the present work. Notably, the significant increase in the average *EDE* values for the leading and trailing wires in mixed mode (L: PMC, T: CMT) and both the wires in CMT mode (L: CMT, T: CMT) are attributed to the possible expansion of the workable WFR range in the advanced short-circuiting (CMT) mode. In summary, Figures 3 and 4 show that the advanced T-GMAW process provides an opportunity to select appropriate metal transfer modes and weld pass parameters for more efficient utilization of the electrical energy to help improve the deposition rate in T-GMAW.

Metallographic evaluation of weld cross-section with inter-layer scanned profiles

Figure 5(a) to (e) shows the top view and the transverse section view at mid-length of the weld coupons for W1 to W5 conditions. The transverse sections are shown with the inter-pass fusion boundaries (in yellow dash line), which are viewed under an optical microscope. A set of corresponding transverse sections is also shown with superimposed laser-scanned deposition profiles (in different coloured lines) after each pass. The weld joint top views exhibit a uniform surface appearance and consistent bead profile without any visible discontinuity for all five welding conditions, indicating a stable deposition with the chosen weaving strategy. The transverse weld cross-sections with the inter-pass fusion boundaries and laser-scanned inter-pass deposition profiles indicate a sound dilution, and adequate groove filling without any lack-of-fusion and other discontinuity.

The transverse weld cross-sections for both W1 and W3 conditions show relatively greater melt pool and deposit volumes, which is attributed to higher energy input with both wires in pulsed (PMC) metal transfer mode. In contrast, the weld cross-sections for the W2, W4 and W5 conditions show relatively smaller melt pool and filler wire deposition with almost the smallest but adequate joint cross-section for the W5 condition with both wires in short-circuiting (CMT) metal transfer mode, minimum energy input amongst all five conditions. The W5 condition could fill the entire groove albeit with no appreciable reinforcement crown. An additional pass to deposit a larger reinforcement crown was avoided for consistency of maintaining six passes for all the welding conditions. The detailed weld joint dimensions for all five conditions are provided in Table S4 of the supplemental document. Overall, Figure 5(a) to (e) shows that all five T-GMAW conditions for different weld parameters produce defect-free multi-pass joints with adequate fusion and groove filling.

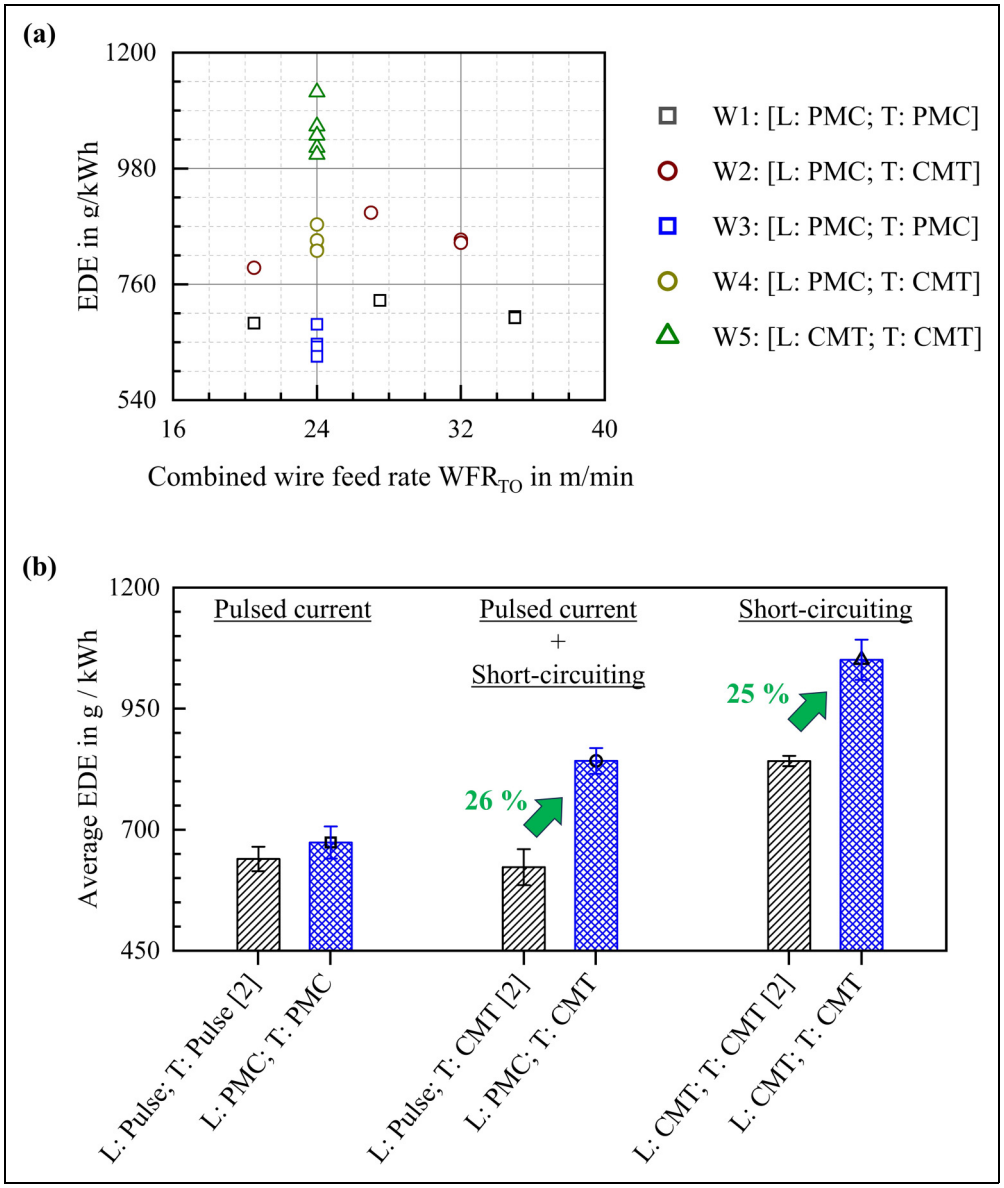

Figure 4. (a) Electrical deposition efficiency (*EDE*) as a function of combined WFR (WFR_{TO}) for second to sixth weld passes for W1 to W5 conditions (Table 1), and (b) comparison of *EDE* in present work with that from literature[2] for T-GMAW. L and T refer to leading and trailing wires.

Inter-layer cooling time $t_{8/5}$ and microhardness mapping

Figure 6(a) presents the measured thermal cycle at mid-length thermocouple locations (TC_2) during six-layer T-GMAW using W3 condition. The thermal cycle associated with each deposited layer is visible as a distinct peak, which increases from the first to sixth pass as the arc moves closer to the thermocouple locations on the top surface. The measured peak temperatures for first to sixth passes are around 180°C, 204°C, 258°C, 302°C, 381°C and 677°C, respectively. A similar layer-wise increase of the peak temperature is noted in Figure 6(b) for all the welding conditions (W1-W5). For W1 and W3 conditions, with both the wires in PMC mode of metal transfer, the peak temperature is greater for W1 due to greater WFR and higher energy input per unit length. Similarly, with the leading wire in PMC mode and trailing wire in CMT mode of metal transfer for both W2 and W4 conditions, the peak temperature is higher for W2 because of higher WFR and greater energy input per unit length. The W5 condition with both wires in CMT mode of metal transfer results in much lower values of peak temperatures for all the passes due to lesser energy input per unit length of weld.

Figure 6(c) shows a sample of the measured cooling curve of the third-layer melt pool at the mid-length during third pass welding for W3 condition and the cooling time ($t_{8/5}$) is extracted around 8.5 s. The melt pool peak temperature could not be measured as it exceeded the thermocouple temperature limit (1200°C). Figure 6(d) shows the measured $t_{8/5}$ cooling time for each pass as a function of the corresponding energy input for W1 to W5 conditions. The values of the energy input for each pass for W1 to W5 conditions are provided in Table S3 in supplemental document. With the deposition moving from the second to sixth pass, the $t_{8/5}$ cooling time increases as the energy input per unit length also increases. For example, the measured cooling time increases from 9.5 s for the second pass to around 28.5 s

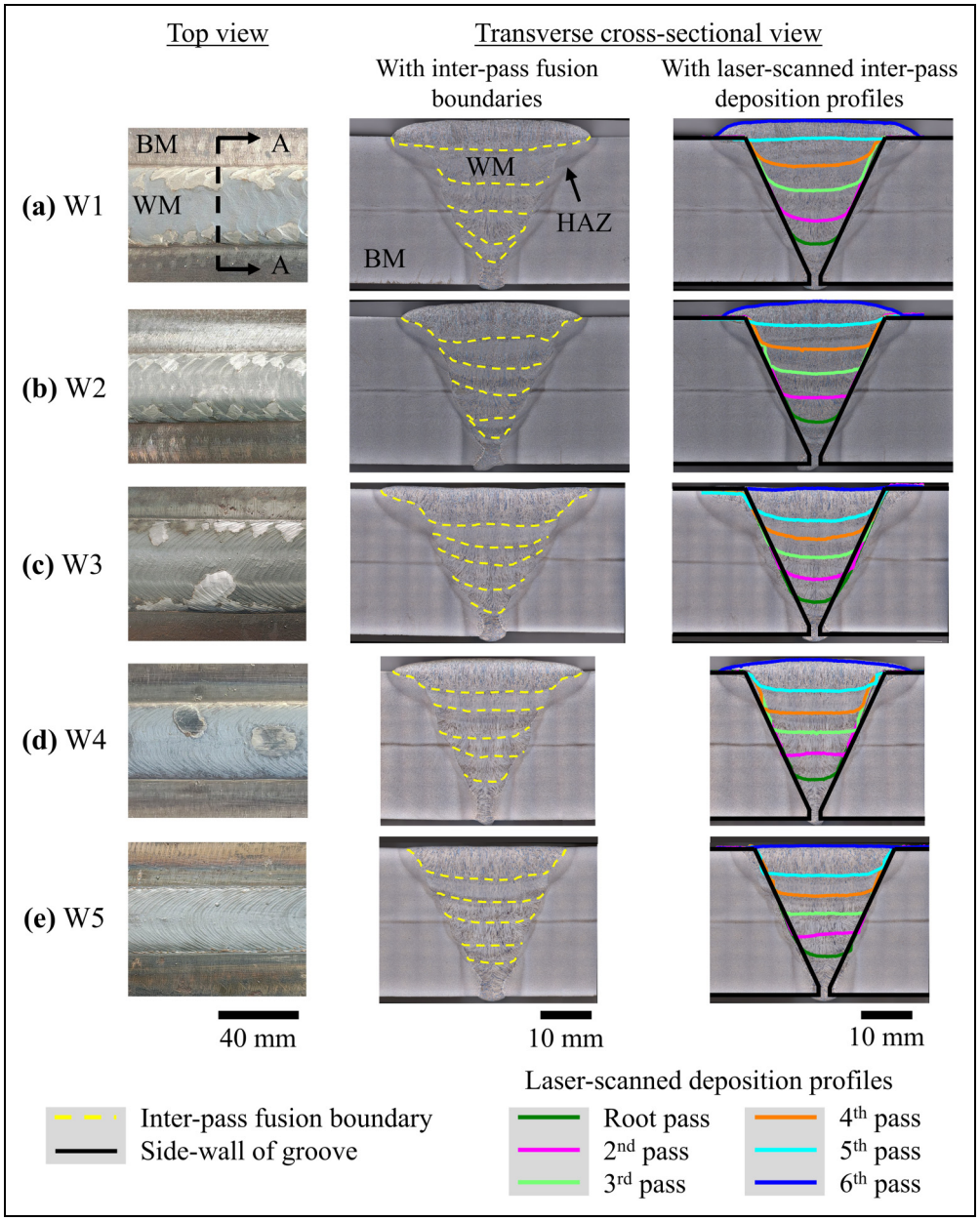

Figure 5. Top view and transverse cross-sectional views of tandem welds with inter-pass fusion boundaries and superimposed laser-scanned profiles for five welding conditions. BM, WM and HAZ refer to the base metal, weld metal, and heat affected zone, respectively.

for the sixth pass for the W1 condition. The corresponding energy input values are 2.01 kJ/mm and 5.29 kJ/mm for the second and sixth passes, respectively. Overall, Figure 6(d) shows that the heat accumulation during multi-pass T-GMAW is influenced by energy input and metal transfer mode. Consequently, the thermal cycles and associated cooling times act as the primary governing factors for the spatial microhardness distribution across the fusion and heat-affected zones.

A grid-based spatial distribution of hardness across the weld joint provides a comprehensive assessment of the joint property in multi-pass weldments. Figure 7(a) shows the split-view representation of weld transverse cross-sections with fusion boundaries (left) and the corresponding spatial microhardness distribution (right) for five conditions. Hardness profiles extracted along the weld width (line A-A) and centreline (line B-B) are plotted in Figure 7(b) and (c), respectively, to quantify the local variations across the fusion zone and HAZ. Figure 7(b) shows the typical hardness variation across the weld width as observed in similar welds,[4] with a relatively higher plateau in the weld metal and gradual decrease toward the HAZ and base metal. In comparison to slightly lower weld zone hardness in W1 and W3 conditions, the welding condition (W5) with short-circuiting mode showed the maximum hardness due to its lower energy input.

Figure 7(c) shows the smooth and comparable hardness variation through thickness across weld centre for all five welding conditions, with little fluctuations for W3 condition, which might be attributed to the cumulative influence of remelting and solidification of previously deposited pass. The measured hardness values for all W1-W5 conditions range from approximately 180–220 HV, which are well within the typical hardness range (150–250 HV) for multi-

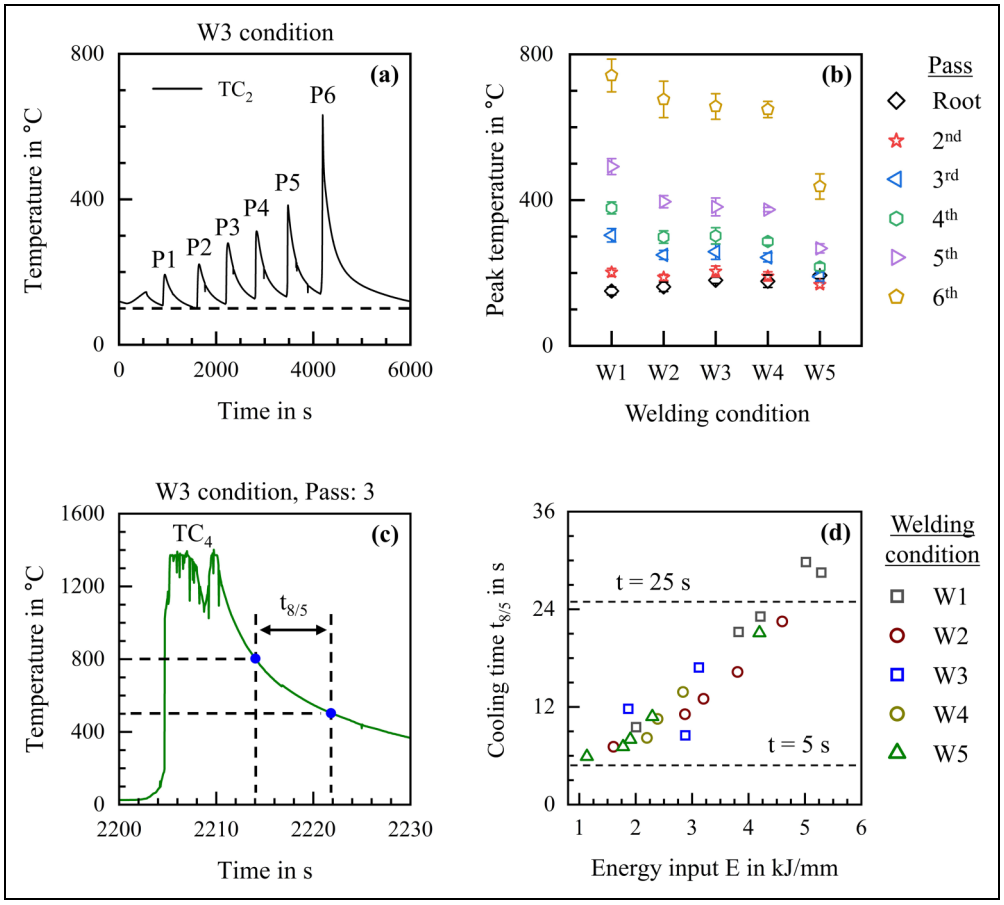

Figure 6. (a) Experimentally measured thermal cycles at mid-length using TC_2 thermocouple (Figure 1c) at W3 condition, (b) layer-wise variation in measured peak temperature for five welding conditions, (c) sample measured cooling cycle of the melt pool using TC_4 thermocouple, and (d) measured critical cooling time ($t_{8/5}$) across different energy inputs per unit length at different welding conditions (Table 1).

pass steel welding. Although the CMT mode of metal transfer (W5) exhibits slightly higher hardness as compared to PMC mode (W1 and W3), these subtle variations are not significant enough to impact joint integrity, especially in thick plate welding. Overall, the spatial hardness mapping demonstrates that the tailored T-GMAW process parameters successfully maintain nearly consistent mechanical property distribution, ensuring the joint integrity required for demanding structural applications. A detailed correlation between the hardness distribution and the underlying microstructural evolution is beyond the scope of the present work and will be addressed in a future investigation.

Summary and conclusions

An integrated and instrumented T-GMAW set-up is used to realize the energy usage vis-à-vis deposition rate for multi-pass welding of a thick steel plate. A novel EDE metric is considered to exhibit as a key performance indicator for T-GMAW, and the effect of different modes of metal transfer and weld pass parameters has been studied in detail. Following are the main conclusions from the present study.

- Compared to the pulse mode, the short-circuiting metal transfer mode offers lower arc power, energy input per unit length, and stable metal transfer, which enables a better control of weld thermal characteristics and subsequent joint properties in multi-pass thick plate welding.
- The *EDE* refers to utilized energy in terms of deposited filler wire mass per kWh of energy consumption. The *EDE* is found notably higher for the short-circuiting metal transfer mode than the pulsed current mode.
- As compared to the lowest EDE around 674 g/kWh for both wires pulse metal transfer mode, the highest EDE around 1051 g/kWh for both wires short-circuiting mode provides an energy-efficient and productive solution for thick plate tandem welding with reduced carbon footprint.
- Compared to pulsed current, the advanced short-circuiting mode reduces the critical cooling time ($t_{8/5}$) to 5–20 s due to lower energy input, which eventually offers greater potential for highly productive tandem welding of high-strength steels.
- The present study provides, for the first time, a substantive basis to evaluate the energy consumption for enhanced metal transfer modes by a quantitative comparison of *EDE*, which also expands the available parameter space in literature for T-GMAW of thick steel plates.

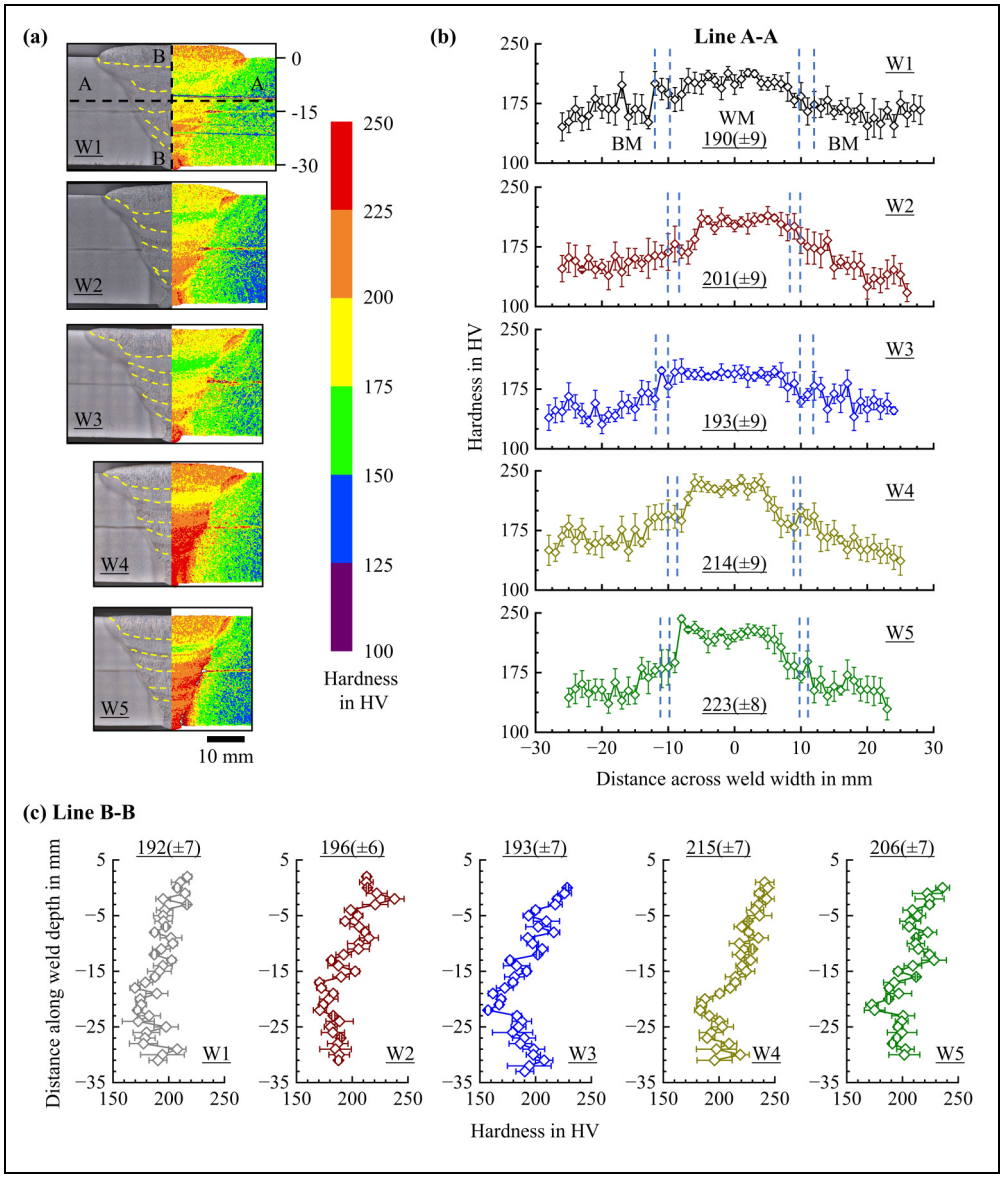

Figure 7. (a) Split-view visualisation of weld cross-sections (W1-W5) with fusion boundaries (left), and Vickers microhardness distribution (right) with profile extraction lines (A-A and B-B), (b) hardness variation across the weld width (A-A line) at 12 mm height, and (c) hardness variation along the weld centreline (B-B line).

Acknowledgements

We gratefully acknowledge the support from Indo-German Science and Technology Centre (IGSTC) Grant 'IGSTC/IF Call 2024/PDIF/PKC-2433/18/2024–25/' for carrying out this work at Bundesanstalt für Materialforschung und –prüfung (BAM), Berlin, Germany. The research project 'SmartWeld – Innovative Design and Manufacturing Concept to Increase the Lightweight Potentials for Steel Construction' was funded by the Federal Ministry for Economic Affairs and Energy (BMWE) under the grant number 03LB2022A. We also sincerely acknowledge Christian Schippereit for his valuable assistance during experiments.

ORCID iDs

Prashant Kumar Chaurasia https://orcid.org/0000-0002-5857-6833
Çağtay Fabry https://orcid.org/0000-0002-0788-8079
Andreas Pittner https://orcid.org/0000-0002-5019-7775
Amitava De https://orcid.org/0000-0002-3109-261X
Michael Rethmeier https://orcid.org/0000-0001-8123-6696

Authors' contributions

P. K. Chaurasia: conceptualization, experimentation, analysis, and writing–original draft. Ç. Fabry: conceptualization, experimentation, analysis, and writing–review and editing. A. Pittner: conceptualization, analysis, and writing–review and editing. A. De: conceptualization and writing–review and editing. M. Rethmeier: conceptualization, writing–review and editing.

Funding

The authors received no financial support for the research, authorship, and/or publication of this article.

Declaration of conflicting interests

The authors declared no potential conflicts of interest with respect to the research, authorship, and/or publication of this article.

Data availability statement

The data can be provided upon request.

Supplemental material

Supplemental material for this article is available online.

References

1. Kim DY, Kim GG, Yu J, et al. Improvement of fatigue performance by applying tandem GMAW in lap joints with gaps. *Int J Adv Manuf Technol* 2023; 128: 2123–2135.
2. Sproesser G, Chang YJ, Pittner A, et al. Environmental energy efficiency of single wire and tandem gas metal arc welding. *Weld World* 2017; 61: 733–743.
3. Sproesser G, Pittner A and Rethmeier M. Increasing performance and energy efficiency of gas metal arc welding by a high power tandem process. *Procedia CIRP* 2016; 40: 642–647.
4. Fang CF, Meng XH, Hu QX, et al. Tandem and GMAW twin wire welding of Q690 steel used in hydraulic support. *J Iron Steel Res Int* 2012; 19: 79–85.
5. Schartner S, Rutzinger B, Soellinger D, et al. Impact of novel arc control mechanisms on the properties of gas metal arc (GMA) tandem welding. *Proc SBW* 2019; 37: 37–49.
6. Krishnan S, Kulkarni DV and De A. Multipass pulsed current gas metal arc welding of P91 steel. *Sci Technol Weld Joining* 2016; 21: 171–177.
7. Kumar PS, Venkaiah N, Basu B, et al. Arc and molten pool behavior on quality of hybrid cold metal transfer and tandem pulsed narrow gap gas metal arc welds: a study. *Mater Manuf Process* 2024; 39: 857–869.
8. Ueyama T, Ohnawa T, Tanaka M, et al. Effects of torch configuration and welding current on weld bead formation in high-speed tandem pulsed gas metal arc welding of steel sheets. *Sci Technol Weld Join* 2005; 10: 750–759.
9. Liu G, Han S, Tang X, et al. Effects of torch configuration on arc interaction behaviors and weld defect formation mechanism in tandem pulsed GMAW. *J Manuf Process* 2021; 62: 729–742.
10. Wu K, Liu Z, Xie P, et al. A comparative study on the bead profile and microstructural characteristics of aluminum alloy welds produced by single and double pulsed tandem gas metal arc welding. *Mater Res Exp* 2019; 6: 0865j1.
11. Li KH, Zhang YM, Xu P, et al. Welding high-strength steel with consumable double-electrode gas metal arc welding process. *Weld J* 2008; 87: 57s–64s.
12. Liu P, Han S, Yi Y, et al. Corrosion behavior of welded joint of Q690 with CMT twin. *Int J Corros* 2018; 1: 2368717.
13. Wu W, Zhao M, Wang H, et al. Twin-wire pulsed tandem gas metal arc welding of API X80 steel linepipe. *Int J Corros* 2018; 1: 7284246.
14. Sprösser G, Chang YJ, Pittner A, et al. Life cycle assessment of welding technologies for thick metal plate welds. *J Clean Prod* 2015; 108: 46–53.
15. Chaurasia PK, Fabry Ç, Pittner A, et al. Automated in situ monitoring and analysis of process signatures and build profiles during wire arc directed energy deposition. *Prog Addit Manuf* 2026; 11: 39–58.
16. Chaurasia PK, Barik BK, Das A, et al. Probing dimensional consistency during multi-track multi-layer gas metal arc directed energy deposition of aluminium alloys. *Weld World* 2024; 68: 925–938.
17. Goecke SF, Syed AA, Ebert-Spiegel M, et al. Probing current, voltage and metal transfer characteristics in pulsed arc and in conventional and a novel low energy input short arc GMAW. *Q J Jpn Weld Soc* 2013; 31: 26s–30s.
18. Das A, Shome M, Goecke SF, et al. Joining of aluminium alloy and galvanized steel using a controlled gas metal arc process. *J Manuf Process* 2017; 27: 179–187.
19. Chaurasia PK, SF G and De A. Real-time monitoring of temperature field, metal transfer and cooling rate during gas metal arc-directed energy deposition. *Sci Technol Weld Joining* 2022; 27: 512–521.
20. Chaurasia PK, SF G and De A. Monitoring melt pool asymmetry in gas metal arc-directed energy deposition. *Sci Technol Weld Joining* 2023; 28: 424–432.
21. Chaurasia PK, SF G and De A. Towards real-time monitoring of metal transfer and melt pool temperature field in gas metal arc directed energy deposition. *Weld World* 2023; 67: 1781–1791.
22. Chaurasia PK, Barik BK, Das A, et al. Evaluating porosity formation in gas metal arc directed energy deposition of an aluminium alloy. *Sci Technol Weld Joining* 2025; 30: 14–24.

Supplemental Document

for

Tandem Gas Metal Arc Welding of Thick Steel Plates: Progress in Productivity and Properties using Advanced Process Modes

S1. Tandem gas metal arc welding (T-GMAW) experimental setup

Figure S1 illustrates a schematic setup embodying the arrangements for real-time monitoring of current, voltage, wire feed rate (WFR) and mode of metal transfer for both the filler wires.

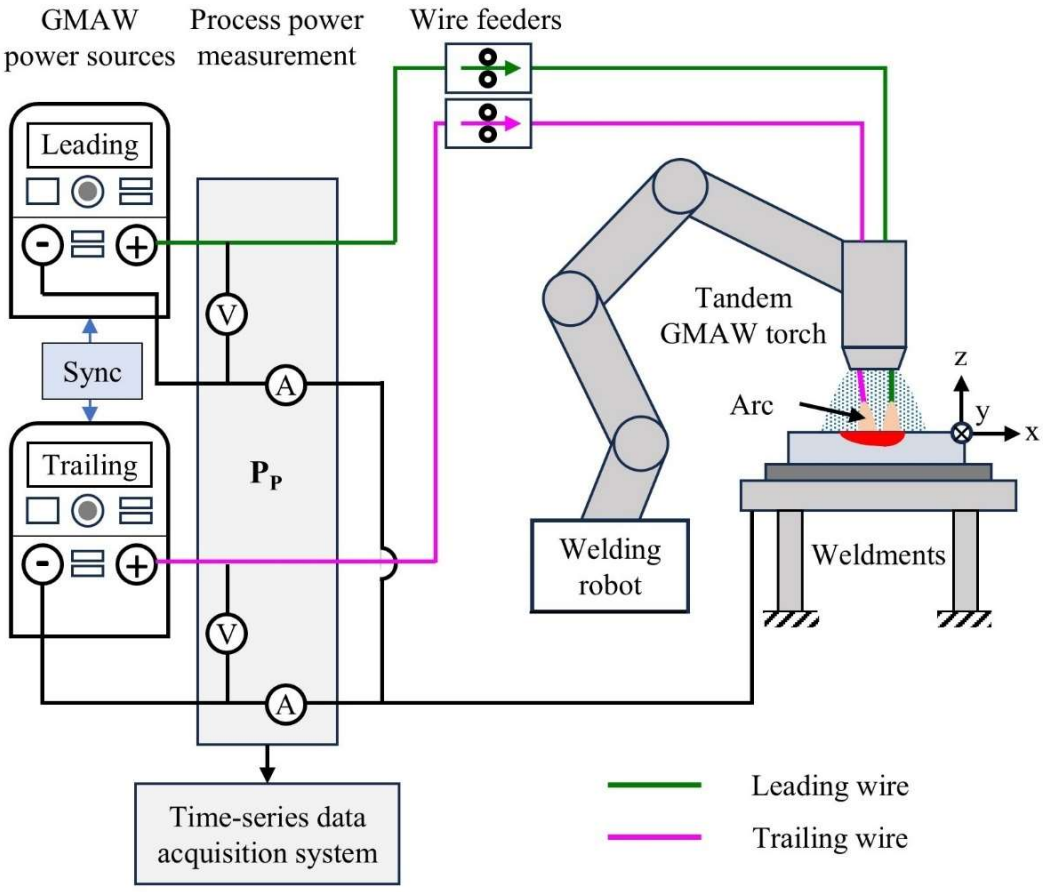

Figure S1 Schematic of tandem gas metal arc welding (T-GMAW) experimental setup with real-time power measurement system [P_P: process (input) power]

To monitor the thermal cycle of the molten pool during welding of each pass, a K-type thermocouple (TC_4) was employed, as shown in Fig. 1(b) in the main text. The thermocouple

was precisely inserted into the trailing edge of the melt pool at the mid-length of the coupon immediately following the passage of the welding arc. This manual insertion technique was standardized to ensure consistent placement across all welding conditions (W1–W5). While the K-type thermocouple allows for high-temperature measurement, the temperature-time history is recorded below 1200°C, which is essential for determining the critical cooling time ($t_{8/5}$) between 800°C and 500°C. This procedure provided a repeatable methodology for correlating the welding process parameters with the resultant thermal history and, subsequently, the mechanical properties of the joints.

S2. Substrate and filler wire materials

Table S1 shows the chemical composition of substrate (355J2+N) and filler wire (AWS A5.18: ER70S-6) materials.

Table S1 Chemical composition (in wt.%) of base material and filler wire as per manufacturer's sheet

	Fe	C	Si	Mn	Cr	Mo	Ni	P	S	Al	Co	Cu	W
Base (Mild steel)	Bal.	0.19	0.22	0.79	0.14	0.02	0.08	0.03	0.02	0.01	0.00	0.19	0.00
Filler wire (ER70S-6)	Bal.	0.08	0.95	1.64	0.03	0.00	0.02	0.01	0.01	0.00	-	0.01	-

S3. List of acronyms and variables

Table S2 presents a combined list of acronyms and variables used in the main text.

Table S2 List of acronyms and variables

List of acronyms		
Abbreviations	**Description**	**Unit**
CMT	Cold metal transfer	-
CTWD	Contact tip to workpiece distance	mm
EDE	Electrical deposition efficiency	g/kWh
GMAW	Gas metal arc welding	-
L	Leading	-
LLT	Laser line triangulation	-
PMC	Pulse multi control	-
SC	Short-circuiting	-
T	Trailing	-
TC	Thermocouple	-
T-GMAW	Tandem gas metal arc welding	-
WTS	Welding travel speed	mm/s
WFR	Wire feed rate	m/min
WFR_L	Leading wire feed rate	m/min
WFR_T	Trailing wire feed rate	m/min
WFR_{TO}	Combined wire feed rate	m/min
2D	Two-dimensional	-
3D	Three-dimensional	-
List of variables		
Symbol	**Nomenclature**	**Unit**
d_W	Diameter of filler wire	mm
E	Energy input per unit length	kJ/mm
E_L	Leading energy input per unit length	kJ/mm
E_T	Trailing energy input per unit length	kJ/mm
EDE	Electrical deposition efficiency	g/kWh
I	Arc current	A
P_P	Process power	kW
P_{PL}	Leading arc power	kW
P_{PT}	Trailing arc power	kW
t	Time	s
v	Welding travel speed	mm/s
v_w	Wire feed rate	m/min
v_{wL}	Leading wire feed rate	m/min
v_{wT}	Trailing wire feed rate	m/min
V	Voltage	V
ρ	Density	g/cm^3

S4. Layer-wise variation in electrical deposition efficiency (EDE)

Table S3 presents the layer-wise process power (P_P), energy input per unit length (E), and electrical deposition efficiency (EDE) for leading (L) and trailing (T) wires, and combined T-GMAW at different welding conditions (W1 – W5).

Table S3 Measured process power (P_P), energy input per unit length (E), electrical deposition efficiency (EDE) for leading (L) and trailing (T) wire feed rates (WFR) during T-GMAW of V-groove butt welds at five different conditions (W1 – W5) [PMC: *Pulse multi control*, CMT: *Cold metal transfer*)

Condition	Layer	WFR_L	P_{PL}	E_L	EDE_L	WFR_T	P_{PT}	E_T	EDE_T	P_P	E	EDE
[L; T]		m/min	kW	kJ/mm	g/kWh	m/min	kW	kJ/mm	g/kWh	kW	kJ/mm	g/kWh
W1: [L: PMC; T: PMC]	1	12.5	9.59	1.44	694.5	-	-	-	-	9.59	1.44	694.3
	2	15	10.51	1.05	760.1	12.5	9.57	0.96	695.8	20.08	2.01	729.5
	3	20	14.04	2.01	758.9	15	12.74	1.82	626.9	26.78	3.83	696.1
	4	20	13.98	2.21	762.0	15	12.70	2.00	629.3	26.68	4.21	698.8
	5	20	13.88	2.60	767.2	15	12.88	2.41	620.3	26.76	5.02	696.6
	6	12.5	9.63	3.21	691.2	8	6.24	2.08	678.4	15.87	5.29	686.2
W2: [L: PMC; T: CMT]	1	12.5	9.57	1.43	695.9	-	-	-	-	9.57	1.43	695.9
	2	15	10.54	1.05	758.3	12	5.52	0.55	1158.8	16.06	1.61	896.1
	3	20	14.02	2.00	759.9	12	6.09	0.87	1039.7	20.11	2.87	844.7
	4	20	14.13	2.23	753.7	12	6.15	0.97	1035.5	20.28	3.20	839.2
	5	20	14.15	2.65	752.7	12	6.15	1.15	1037.6	20.30	3.81	838.9
	6	12.5	9.55	3.18	697.0	8	4.24	1.41	1004.2	13.79	4.60	791.5
W3: [L: PMC; T: PMC]	1	12	9.57	1.44	667.9	-	-	-	-	9.57	1.44	667.7
	2	12	8.91	0.89	717.4	12	9.78	0.98	653.6	18.69	1.87	684.0
	3	12	9.99	1.43	668.8	12	10.30	1.47	602.4	20.29	2.90	629.8
	4	12	9.27	1.46	688.6	12	10.49	1.66	609.3	19.76	3.12	646.5
	5	12	9.35	1.75	682.9	12	10.58	1.98	604.2	19.93	3.74	641.1
	6	12	9.78	3.26	653.3	12	10.73	3.58	595.7	20.51	6.84	623.2
W4: [L: PMC; T: CMT]	1	12	9.54	1.43	669.6	-	-	-	-	9.55	1.43	669.4
	2	12	8.94	0.89	704.6	12	5.59	0.56	1144.1	14.53	1.45	873.7
	3	12	9.55	1.36	668.6	12	5.84	0.83	1083.3	15.39	2.20	826.1
	4	12	9.28	1.46	687.1	12	5.85	0.92	1091.8	15.13	2.39	843.6
	5	12	9.27	1.74	688.3	12	5.87	1.10	1088.3	15.14	2.84	843.5
	6	12	9.60	3.20	665.1	12	5.86	1.95	1083.8	15.46	5.15	823.8
W5: [L: CMT; T: CMT]	1	12	9.47	1.42	674.5	-	-	-	-	9.48	1.42	674.3
	2	12	5.59	0.56	1144.4	12	5.77	0.58	1106.2	11.35	1.14	1125.0
	3	12	6.22	0.89	1039.1	12	6.22	0.89	1001.4	12.44	1.78	1019.7
	4	12	5.97	0.94	1076.2	12	6.10	0.96	1044.9	12.06	1.90	1060.4
	5	12	6.05	1.13	1056.6	12	6.19	1.16	1029.5	12.24	2.29	1042.9
	6	12	6.22	2.07	1024.2	12	6.36	2.12	989.2	12.58	4.19	1006.6

S5. Measured weld dimensions

Table S4 presents the measured weld dimensions and dilution percentage for all five welding conditions (W1 to W5).

Table S4 Measured weld dimensions and dilution (%) for all five conditions (W1-W5)

Welding condition	Leading (L) and trailing (T) wires mode	Weld width	Weld reinforcement height	Dilution
		mm	mm	%
W1	L: PMC; T: PMC	39.34(±0.5)	3.51(±0.4)	12
W2	L: PMC; T: CMT	35.38(±0.2)	3.09(±0.3)	5
W3	L: PMC; T: PMC	42.66(±0.4)	0.67(±0.5)	23
W4	L: PMC; T: CMT	37.80(±0.3)	1.90(±0.5)	13
W5	L: CMT; T: CMT	35.53(±0.6)	0.42(±0.5)	16